#572

SIX

Oxygen Chemisorption Effects on Graphite Thermoelectric Power

P. L. WALKER, JR., L. G. AUSTIN, and J. J. TIETJEN

Fuel Science Department, The Pennsylvania State University
University Park, Pennsylvania

I. Introduction

Although the electronic properties of carbons and graphites have been studied extensively in the past two decades (1–4), comparatively little attention has been given to the thermoelectric power of graphite, particularly from the theoretical point of view. This is partly because of the difficulty in obtaining homogeneous graphitic systems of high purity that have sufficient size to be suited to thermoelectric studies. In addition, the absence of a theory with which to correlate experimental findings has undoubtedly presented a serious obstacle to extensive investigation of this subject. It is not surprising, therefore, that the effect of chemisorbed gases on the thermal emf of graphite has practically been ignored, even though graphite is an ideal material on which to conduct such a study. That is, as will be discussed in Section III, graphite has a unique π-electron band structure, of which the positive and negative carriers are balanced closely in concentration and the total carrier concentration is small (*ca.* 10^{18}/cc solid) relative to metals. These factors cause the thermoelectric power to be very sensitive to any process which results in the trapping of negative carriers—for example, as will be seen, the chemisorption of oxygen.

The literature is replete both with investigations of oxygen chemisorption on carbons to form an oxygen complex and with the importance of the chemisorption on the surface properties of carbons. Notable reviews of this subject have been given by Smith (5) and Culver and Watts (6). Surprisingly, in spite of all the studies there have been virtually no papers reporting quantitative results on the kinetics of oxygen chemisorption. Generally speaking, when carbon is exposed to oxygen three products can form: gaseous carbon monoxide, gaseous carbon dioxide, and a carbon-oxygen surface complex. The amount of gaseous products formed relative to the amount of complex formed is strongly dependent upon temperature. At sufficiently low temperatures, the complex is formed almost exclusively. For example, Laine and co-workers (7) have shown that oxygen chemisorbs on highly purified carbon at temperatures at least as low as 300° C, while the production of gaseous products is negligible. As temperature is increased, the rate of complex formation increases and also at some temperature the rate of gaseous product formation becomes significant. For high-purity carbons, gaseous product formation becomes significant at about 500° C and increases at a rate which shows an activation energy around 44 kcal/mole with increasing temperature (8). Also around 500° C the rate of complex breakdown becomes significant; and since its rate has a greater temperature dependence than does the rate of oxygen chemisorption, the amount of surface complex decreases with further increases

in temperature. Finally, around 950° C there is virtually no surface oxygen complex remaining.

The presence of an oxygen complex on the surface of carbons and graphites has profound effects (sometimes desirable and sometimes undesirable) on the performance of these materials in practical applications. Probably the most striking example of the importance of oxygen chemisorption on carbons and graphites is related to the effect of the presence of an oxygen atmosphere on the behavior of brushes in motors. Under high vacuum, carbon is a poor lubricant and extensive "wear-dust" can form (9,10). In the presence of 300 torr of oxygen, carbon wear rate is reduced close to zero (11). It is suggested that oxygen chemisorbs on the carbon, producing hydrophilic sites for the physical adsorption of clusters of water molecules. These clusters serve as "spacers" between the carbon and the moving face to prevent wear. Recently, it has been shown that the extent of hydrophobicity of a graphitized carbon black, which is a function of the amount of chemisorbed oxygen, is quite critical in determining the success of the black to nucleate ice crystals (12). This is of importance when carbons are used in the seeding of clouds to produce rain or snow.

The initial presence of oxygen complex on carbon blacks determines whether a strong, consolidated body can be produced by compaction of the black, in the absence of a binder phase (13). If a carbon black containing chemisorbed oxygen is first compacted at pressures around 400 atm and then heated to approximately 1000° C, a body of good strength is produced. It is suggested that heating the black removes oxygen complexes, producing active sites (location of unpaired electrons) on adjacent particles which bond the particles together.

Zelinski (14) showed that oxygen complexes, possessing predominately either oxidizing or reducing characteristics, can be formed on graphite depending upon the oxygen pressure and temperature. Graham (15) showed that activated carbon surfaces, having different amounts of oxidizing and reducing oxygen complex present, vary markedly in their adsorption capacity of acidic and basic adsorbates of similar size.

Surface oxygen complexes play an important role in determining the behavior of carbon blacks in rubber. Blacks with a high concentration of surface oxygen will yield a rubber product which ages rapidly and has a high electrical resistance (5). When carbon blacks are used in the formulations of inks and paints, the extent of surface oxygen complex affects the flow and suspension stability of the material (16).

Graphite is widely used today as a moderator in nuclear reactors (17). However, the presence of chemisorbed oxygen on the graphite is of serious concern. When the reactor is brought to operating temperature, the complex which formed during the graphite manufacture and/or in the

reactor in the presence of impure coolant gas (helium) is released primarily as carbon monoxide. The carbon monoxide disproportionates over steel heat exchanger tubes and structural members causing undesirable metal carburization.

In this chapter the authors have attempted to supply references to the majority of pertinent papers on the thermoelectric power of carbons and graphite. A theory of the thermoelectric power of graphite, based on an application of the general principles of transport phenomena in solids, has been developed. This theory has been used to aid in the understanding of experimental results obtained on the effect of oxygen chemisorption on the thermoelectric power of graphite. The kinetics of oxygen chemisorption on pure graphite and graphite containing iron have been followed by thermoelectric power changes. From the magnitude of the preexponential term in the rate constant for oxygen chemisorption, information has been obtained on the nature of the activated complex leading to oxygen chemisorption.

II. Review of Previous Thermoelectric Power Studies on Graphite and Carbons

The earliest reported values of the thermoelectric power of carbon (18–22) show large differences in magnitude and temperature dependence. LaRosa (23), in reviewing these early investigations, attributed the observed discrepancies to experimental difficulty and variation in sample purity. In an effort to avoid the latter problem, he heated a carbon rod at approximately 800° C in a chlorine atmosphere for nine hours. This treatment reduced the ash content (primarily iron and silicon dioxide) to 0.07 per cent and yielded a specimen having a positive thermoelectric power, relative to platinum, which increased linearly with increase in ambient temperature. Since these observations were not in agreement with any of his predecessors, LaRosa concluded that because of the purity of his samples his results represented the true values of the thermoelectric power of carbon. It should be noted, however, that the disagreement in the published values might have been due to variations in the crystal structure of the carbons examined, rather than to the presence of impurities. In fact it is possible that chlorine may have chemisorbed on the carbon surface during the purification process and had a pronounced effect on LaRosa's measurements. One can only conclude that in examining thermoelectric effects, as with all other electronic properties, it is extremely important to carefully characterize the system being studied.

Hukuda and Saito (24) measured the thermoelectric power of graphitic and turbostratic carbon films produced *in vacuo* by the thermal

decomposition of a number of aliphatic hydrocarbons. They found the thermoelectric power to be negative with respect to copper, becoming more negative as the ambient temperature was increased. They also reported that adjusting the experimental conditions, so as to facilitate large crystal growth and high carbon content, produced films having values approaching that of graphite.

Tyler and Wilson (25) examined the thermoelectric power, relative to copper, of graphitized, extruded rods made from petroleum coke and pitch; graphitized, molded rods made from natural graphite and pitch; and graphitized, molded rods made from lampblack and pitch over the temperature interval 20° K to 280° K. After converting their data to absolute values, they found that the thermoelectric power of the lampblack rods was positive and increased monotonically with increase in temperature, while the other samples had negative values which passed through a minimum below 50° K. The authors, citing the absence of a theory for the thermoelectric power of carbon or graphite, were unable to interpret their results.

In an attempt to study the effect of induced structural defects, Eatherly and Razor (26) investigated the thermoelectric power of nine grades of artificial and natural graphites which were exposed to varying amounts of neutron irradiation. Their measurements were restricted to the temperature region 4° K to 300° K. In qualitative agreement with Tyler and Wilson, Eatherly and Razor found that most of their samples had negative thermoelectric power values which exhibited a minimum below 100° K. Increased neutron exposure raised the thermoelectric power until eventually a positive value was obtained. This change was attributed to the effect of dislocated atoms acting as interstitial acceptor states which remove electrons from the conduction band and increase the relative number of positive holes.

Kmetko (27) formed bisulphate compounds by oxidizing carbons in sulphuric acid and observed that the thermoelectric power of these materials became more positive with increased oxidation. He ascribed this effect to a removal of electrons from the conduction band as a result of electrostatic repulsion by the bisulphate ions. It is possible, however, that the formation of lamellar compounds may affect the electronic properties of the parent material simply by distorting the crystal lattice. In fact, Kmetko reported that the increase in the thermoelectric power was greater in the case of residue compounds than for the corresponding lamellar compounds. This suggests that the actual mechanism involves more than just a change in the number of current carriers.

The thermoelectric power of both soft and hard cokes was examined by Loebner (28) as a function of heat treatment from 1000° C to 3100° C.

He observed that the absolute thermoelectric power values were positive and decreased slightly to a flat minimum at 1400° C, increased to a maximum at 2100° C, and then decreased until they became negative at the highest heat treatment temperatures. The explanation of this phenomena was based on a model proposed by Mrozowski (29). According to this model, the initial decrease results from an increase in the number of positive holes as π electrons are trapped in vacant σ orbitals on the periphery of crystallite planes. The increase in the thermoelectric power from 1400° C to 2100° C results from a decrease in the number of peripheral sites upon crystal growth, and the final decrease above 2100° C arises from an increase in the number of electrons thermally excited into the conduction band as the energy gap decreases for the more graphitic materials. This explanation relies on assuming a one-band model for low heat-treated materials which converts to a two-band model at higher heat-treatment temperatures.

Ubbelohde and Orr (30) measured the thermoelectric power of an *a*-axis, *c*-axis graphite thermocouple and observed that the thermal emf increased linearly with temperature up to 700° C. Above this temperature the thermoelectric power began to decrease, which the authors attributed to oxidation of the thermocouple. They suggested that oxygen might form a quinone structure which removes electrons from the cooperative aromatic system (thereby raising the work function of the *a*-axis substance) and reduces the thermal emf between the two materials.

In order to properly characterize the anisotropy, Blackman, Dundas, and Ubbelohde (31) investigated the thermoelectric power as a function of crystallographic direction of a variety of graphite specimens. These included extruded polycrystalline graphite partially oriented during its manufacture, pyrolytic graphite, flakes of natural graphite oriented by compression, and natural graphite having good columnar orientation parallel to the *a*-axis. Potassium- and bromine-graphite crystal compounds were prepared for the purpose of producing changes in the concentration of electrons or positive holes. The results of these experiments and those of resistivity determinations were correlated with the thermoelectric power measurements. Their findings accord with the view that in ideal graphite conduction in the *a*-axis direction is primarily by electrons, while in the direction of the *c*-axis conductance by positive holes predominates. This consideration is based primarily on the fact that a correlation was obtained between the specific resistance and the thermoelectric power. The correlation is such that for resistivity values corresponding to *a*-axis oriented near-ideal graphite the thermoelectric power is negative, while it is positive in the corresponding *c*-axis case. Also, using the specific resistance as a measure of the degree of crystalline perfection indicates that crystal defects

serve as electron traps which cause the thermoelectric power to become more positive as the degree of crystal perfection decreases. This conclusion is supported by the fact that increasing the electron concentration by forming potassium-graphite crystal compounds caused both the *a*-axis and *c*-axis thermoelectric power values to become more negative; whereas the reverse effect was observed in the case of bromine-graphite formation.

Blackman, Saunders, and Ubbelohde (32) prepared a series of pyrolytic carbons by decomposing methane at temperatures ranging from 1600° C to 2200° C. They observed that specimens formed at the higher deposition temperatures had lower resistivity and thermoelectric power values. In agreement with Loebner and Mrozowski, the authors concluded that at low temperatures of formation the trapping of electrons in surface states leads to a preponderance of positive holes producing a single carrier system. At methane-decomposition temperatures ranging from 1600° C to 1900° C, the thermoelectric power was found to be a linear function of measurement temperature between 77° K and 293° K. As the degree of graphitization was increased the thermoelectric power eventually became negative, and the most graphitic specimens showed what the authors termed anomalies at low temperatures (0° K to 100° K). These materials exhibited a pronounced minimum in the temperature region 85° K to 90° K and underwent sign reversals. The authors suggested that these low temperature effects may be due to "Umklapp-Prozesse" or phonon drag effects, and in less graphitic substances these anomalies are suppressed owing to a smaller mean free path of both charge carriers and phonons. This concept was supported by the fact that distorting the lattice of a well-graphitized material by the formation of $C_{362}Br$ restored the linear temperature dependence at the low temperatures.

Klein and Lepie (33) investigated the output and sensitivity of thermoelectric devices where one element consisted of high-purity pyrolytic graphite (PG) and the other element consisted of boron-doped pyrolytic graphite (PGB). It is known that boron atoms go into substitutional trigonal sites in the graphite lattice and act as electron acceptors. It was concluded that PGB/PG thermocouples, when operated below 2000° C and protected from chemical attack, offer some valuable advantages over existing high-temperature devices. The output is greater than most other material combinations, being at least twice that generated by thermocouples of the tungsten/tungsten-rhenium variety, for example. The system PG/0.7% B-PG was found to warrant particular attention since the output increases nearly linearly with temperature, while producing a sizeable output of 75 mV at 2000° C. The sensitivity of the couple is also large, with a thermoelectric power of about 50 μV/°C at 1000° C. Output instability problems were eliminated by an annealing treatment of both

thermoelements around 2900° C prior to initial heating of the PGB/PG combination.

Recently, Klein (34) has examined the behavior of the Seebeck-coefficient of pyrolytic graphites in terms of the general theory of narrow-band semiconductivity and the simple two-band model, for temperatures below 300° K. He concludes that the temperature dependence of the thermoelectric power may be accounted for on the basis of a difference in the relative temperature dependence of the electron and hole mobilities.

III. A Theory of the Thermoelectric Power of Graphite

A theory of the thermoelectric power of graphite has not been formulated to date. Therefore, in order to interpret the experimental findings of this investigation, the ensuing discussion is presented to furnish a description of the thermal emf in graphite. It is based on an application of the general principles of transport phenomena in solids (35,36,37), as they pertain to thermoelectric effects, to a relatively simple model of the electronic energy band structure and scattering mechanism for polycrystalline graphite.

There exist a number of phenomenological laws which may be expressed in the form of proportionalities between a current of some species and a gradient of some physical parameter, or so-called generalized force (38). These phenomena can occur simultaneously when more than one potential is present at the same time, and in the most general case any generalized force can give rise to any current. The mathematical statement of this fact is

$$\mathbf{J}_i = \sum_{j=1}^{n} L_{ij}\mathbf{X}_j \qquad (i = 1, 2, \ldots n) \qquad \text{(Eq. 1)}$$

where $\mathbf{J}_i$ $(i = 1, 2, \ldots n)$ are the currents, $\mathbf{X}_j$ $(j = 1, 2, \ldots n)$ are the forces, L_{ij} $(i, j = 1, 2, \ldots n)$ are termed the phenomenological coefficients, and the bold-faced symbol indicates a vector quantity. The specific set of such equations that apply to the case of thermoelectric phenomena are those involving the flow of electrical and thermal currents and the gradients of temperature and electrical potential. That is,

$$\mathbf{J}_1 \equiv \mathbf{J} = L_{11}\mathcal{E} + L_{12}\nabla T \qquad \text{(Eq. 2)}$$

$$\mathbf{J}_2 \equiv \mathbf{Q} = L_{21}\mathcal{E} + L_{22}\nabla T \qquad \text{(Eq. 3)}$$

where $\mathbf{J}$ is the electrical current per unit volume, $\mathbf{Q}$ is the thermal flux per unit volume, $\mathcal{E}$ is the electrical field, and ∇T is the thermal gradient. It

follows from equation (2) that there exists a dependent electric field in the presence of an impressed thermal gradient, under the condition that the charge flux be zero. That is,

$$\mathscr{E} = -\frac{L_{12}}{L_{11}}\nabla T \equiv \alpha \nabla T \qquad \text{(Eq. 4)}$$

where α is the thermoelectric power. Therefore, a discussion of the thermoelectric power should properly begin by considering the electrical current per unit volume (39),

$$\mathbf{J} = \frac{1}{4\pi^3}\int e\mathbf{v}(\mathbf{K})\, f(\mathbf{K}, \mathbf{r}, t)\, d\mathbf{K} \qquad \text{(Eq. 5)}$$

where e is the electronic charge, $\mathbf{v}$ is the electron velocity, f is the non-equilibrium distribution function, $\mathbf{K}$ is the momentum or wave vector, $\mathbf{r}$ is the position vector, t is the time, and the integration is carried out over all of momentum space. The problem reduces in principle to obtaining the proper distribution function f, performing the integration indicated in equation (5), setting $\mathbf{J}$ equal to zero, and solving for α as in equation (4).

In order to obtain the proper expression for f it is necessary to consider the Boltzmann transport equation, which in terms of the variables introduced in equation (5) is

$$\frac{\partial f}{\partial t} + \dot{\mathbf{K}} \cdot \nabla_K f + \mathbf{v} \cdot \nabla_r f = \left[\frac{\partial f}{\partial t}\right]_{\text{coll}} \qquad \text{(Eq. 6)}$$

The term on the right-hand side of equation (6) accounts for time variations of the distribution function which arise from interactions of the system (conduction electrons) in the form of scattering processes. The complexity of this term introduces the greatest difficulty to an exact solution of the Boltzmann equation. Therefore, it is useful to consider a relaxation time approximation (40), wherein

$$\left[\frac{\partial f}{\partial t}\right]_{\text{coll}} = \frac{f_0 - f}{\tau} \qquad \text{(Eq. 7)}$$

for f_0 the equilibrium, or Fermi-Dirac, distribution function and τ a characteristic relaxation time. Then the scattering processes are characterized such that a disturbance from equilibrium, caused by collisions, is one in which the system undergoes an exponential decay back to equilibrium according to a characteristic time τ. This follows from the fact that the

solution to equation (7) is

$$f = f_0[1 - \exp(-t/\tau)] \qquad \text{(Eq. 8)}$$

The reciprocal of the relaxation time is a measure of the probability for scattering (41), and should be a composite term for a system of compacted, polycrystalline graphite. That is,

$$\frac{1}{\tau} = \sum_{i=1}^{3} \frac{1}{\tau_i} \qquad \text{(Eq. 9)}$$

where the subscripts 1, 2, and 3 refer to phonon, crystallite boundary, and particle boundary scattering, respectively. The Boltzmann equation may be made linear by assuming that

$$\nabla_K f = \nabla_K f_0 \qquad \text{(Eq. 10)}$$

and

$$\nabla_r f = \nabla_r f_0 \qquad \text{(Eq. 11)}$$

which is a good assumption if the impressed thermal gradient is kept small and, therefore, the system is not far removed from equilibrium. The time variation of the wave vector $\mathbf{K}$ is (42)

$$\dot{\mathbf{K}} = \frac{e\mathscr{E}}{\hbar} \qquad \text{(Eq. 12)}$$

where $\hbar$ is Planck's constant divided by 2π. Also

$$\nabla_K f_0 = \hbar \mathbf{v} \frac{\partial f_0}{\partial E} \qquad \text{(Eq. 13)}$$

for E the electron energy, since

$$\nabla_K f_0 = \frac{\partial f_0}{\partial E} \nabla_K E \qquad \text{(Eq. 14)}$$

and (43)

$$\mathbf{v} = \frac{1}{\hbar} \nabla_K E \qquad \text{(Eq. 15)}$$

The gradient, with respect to position, of the equilibrium distribution function depends on both the temperature and the chemical potential, or Fermi energy μ. That is,

$$\nabla_r f_0 = \frac{\partial f_0}{\partial T} \nabla_r T + \frac{\partial f_0}{\partial \mu} \nabla_r \mu \qquad \text{(Eq. 16)}$$

However,

$$\frac{\partial f_0}{\partial T} = -\frac{(E-\mu)}{T} \frac{\partial f_0}{\partial E} \qquad \text{(Eq. 17)}$$

and

$$\frac{\partial f_0}{\partial \mu} = -\frac{\partial f_0}{\partial E} \qquad \text{(Eq. 18)}$$

Therefore, by suitably combining equations (7), (10), (11), (12), (13), (16), (17), and (18), f may be obtained from equation (6). The result under steady state conditions is

$$f = f_0 - \tau \mathbf{v} \cdot \left[e\mathscr{E} - \nabla_r \mu - \frac{(E-\mu)}{T} \nabla_r T \right] \frac{\partial f_0}{\partial E} \qquad \text{(Eq. 19)}$$

Substitution of equation (19) in equation (5) yields

$$\mathbf{J} = -e^2 I_0 \mathscr{E}' + \frac{e}{T} I_1 \nabla_r T \qquad \text{(Eq. 20)}$$

where the effective electric field is

$$\mathscr{E}' = \mathscr{E} - \frac{1}{e} \nabla_r \mu \qquad \text{(Eq. 21)}$$

and

$$I_n = \frac{1}{4\pi^3} \int v^2 \tau (E-\mu)^n \frac{\partial f_0}{\partial E} \, d\mathbf{K} \qquad \text{(Eq. 22)}$$

Equation (22) may be expressed as an integral over the energy and becomes

$$I_n = \frac{1}{4\pi^3} \int v^2 \tau (E-\mu)^n \frac{\partial f_0}{\partial E} \frac{dS}{|\nabla_K E|} \, dE \qquad \text{(Eq. 23)}$$

where dS is a differential element of area on a surface of constant energy E.

It is necessary to evaluate the integrals I_n, each of which contain a derivative, with respect to the energy, of the Fermi-Dirac distribution function. This derivative is a highly peaked function having nonzero values only within a limited region about the Fermi energy and approaches a Dirac delta function as the degree of degeneracy of the electronic system increases. In the limit of complete degeneracy, the values of these integrals could be determined by evaluating their integrands at the Fermi surface. However, since the charge carriers in graphite are only partially degenerate, it is necessary to expand the integrands of I_n in a Taylor series about $E = \mu$ and evaluate the integrals as specific sums. That is, if

$$I_n \equiv \int G_n(E) \frac{\partial f_0}{\partial E} \, dE \qquad \text{(Eq. 24)}$$

and

$$G_n(E) \equiv g(E)(E - \mu)^n \qquad \text{(Eq. 25)}$$

where

$$g(E) = \frac{1}{4\pi^3} \int \frac{v^2 \tau \, dS}{|\nabla_K E|} \qquad \text{(Eq. 26)}$$

then

$$G_n(E) = \sum_m \frac{\partial^m G_n(E)}{\partial E^m}\bigg|_{E=\mu} \frac{(E - \mu)^m}{m!} . \qquad \text{(Eq. 27)}$$

Therefore, to a second order approximation

$$I_n = \int \left[G_n(E)\Big|_{E=\mu} + \frac{\partial G_n(E)}{\partial E}\bigg|_{E=\mu} (E - \mu) + \frac{\partial^2 G_n(E)}{\partial E^2}\bigg|_{E=\mu} \frac{(E - \mu)^2}{2} \right] \frac{\partial f_0}{\partial E} \, dE \qquad \text{(Eq. 28)}$$

and the terms in this sum may be evaluated individually (44). The result is

$$I_0 = -g(E)\Big|_{E=\mu} \qquad \text{(Eq. 29)}$$

and

$$I_1 = -\frac{\pi^2 k_B{}^2 T^2}{3} \frac{\partial g(E)}{\partial E}\bigg|_{E=\mu} \qquad \text{(Eq. 30)}$$

where k_B is the Boltzmann constant. It should be noted that the expansion of the integrands of I_n is arbitrarily limited to a second order

approximation, even though the precise degree of degeneracy of the electronic system is unknown. However, as will be seen in Section IV, limiting the expansion in this manner results in a final expression for the thermoelectric power which has the proper temperature dependence, while including additional terms in the expansion would introduce a temperature dependence other than that observed experimentally.

It follows from equations (2), (4), and (20) that

$$\alpha = \frac{I_1}{eTI_0} \qquad \text{(Eq. 31)}$$

which, because of equations (29) and (30), becomes

$$\alpha = \frac{\pi^2 k_B{}^2 T}{3e}\left[\frac{\partial}{\partial E}\ln\left(\frac{1}{4\pi^3}\int\frac{\tau v^2\,dS}{|\nabla_K E|}\right)\right]_{E=\mu} \qquad \text{(Eq. 32)}$$

However, since the density of states $N(E)$ is given by (45)

$$N(E) = \frac{1}{4\pi^3}\int\frac{dS}{|\nabla_K E|} \qquad \text{(Eq. 33)}$$

and the evaluation of the term in brackets, in equation (32), is limited to $E = \mu$, for a system such as graphite, which involves more than one energy band, α becomes

$$\alpha = \frac{\pi^2 k_B{}^2 T}{3e}\left[\frac{\partial}{\partial E}\ln\left(\sum_i N_i\tau_i v_i^2\right)\right]_{E=\mu} \qquad \text{(Eq. 34)}$$

Here, the summation is over the discrete energy bands and allows the evaluation of the term in brackets to be made over the entire Fermi surface.

The actual energy band structure of graphite has been determined, in great detail, by a number of workers (46). The major results of these calculations, pertinent to this discussion, are twofold. First the valence and conduction bands overlap, and second the constant energy contours near the corners of the Brillouin zone take the form of ellipsoids for both electron and positive hole states. The complete mathematical expression for this description is quite complicated and it is not at all certain that the accurate detail of this complex model would either be required or substantially contribute to a discussion of transport phenomena in a polycrystalline material. Therefore, a much simpler approach is taken here by

approximating the ellipsoidal energy contours by cylindrical energy surfaces having the form

$$E_p = \Delta - \frac{\hbar^2}{2m_p}(K_x^2 + K_y^2) \qquad \text{(Eq. 35)}$$

and

$$E_e = \frac{\hbar^2}{2m_e}(K_x^2 + K_y^2) \qquad \text{(Eq. 36)}$$

The subscript e refers to electrons, while p refers to positive holes, m is the effective mass, Δ is the band overlap, and K_x and K_y are the x and y components of the wave vector, respectively.

This approximation is particularly well suited to the systems employed in this study. That is, in conjunction with the graphite sample preparation (discussed in Section IV) an examination was undertaken to determine the effect on the thermoelectric power values of variations in the molding pressure P_m and the rate of application of the pressure, R_m. It was observed that a negligible effect was produced by varying these parameters within broad limits about the sample preparation values (P_m = 100,000 psi; R_m = 750 psi/sec). In this investigation, the values of P_m ranged from 25,000 psi to 125,000 psi and R_m varied from 500 psi/sec to 1000 psi/sec.

It is known that the thermoelectric power of graphite is highly anisotropic and that crystallite or particle orientation in compacted graphite samples is affected by molding pressure (31). Also, it has been observed that when natural graphite flakes are compacted the resulting specimens exhibit a high degree of crystallite alignment with the a-axis oriented perpendicular to the pressing direction (47). Therefore, it may be concluded that with the sample preparation conditions utilized in this study a sufficient degree of crystallite alignment has been achieved so that the resulting systems may be approximated as having a thermal gradient impressed along the a crystallographic dimension. In the limit that this alignment were made perfect, the energy band structure as derived from a two-dimensional model of graphite would become appropriate (48). However, under such conditions the more precise, ellipsoidal energy contours and the approximate, cylindrical type reduce to a common circular form.

It has been found in examining the theory of the electrical resistivity of graphite that it is adequate to consider the relaxation time to be energy-independent (49). If this assumption is made here, the final expression for the thermoelectric power may be obtained from equation (34). The energy dependence of the remaining parameters which comprise equation (34) is

determined as a result of equations (35) and (36). The result is

$$\alpha = \frac{\pi^2 k_B^2 T}{2e}\left[\frac{n_e\tau_e/m_e\mu - n_p\tau_p/m_p(\Delta-\mu)}{n_e\tau_e/m_e + n_p\tau_p/m_p}\right] \qquad \text{(Eq. 37)}$$

where since the terms included in the brackets of equation (37) are evaluated at the Fermi surface, the density of states has been replaced by the number of carriers n_e and n_p. Although it has been assumed that the relaxation time is energy-independent, this is not necessary in order that the final expression for the thermoelectric power be essentially that of equation (37). As long as the energy dependence of the relaxation time has the general form, $\tau = \tau_0 E^q$, for q any real number, the final expression for the thermoelectric power will differ from equation (37) only by a multiplicative constant.

With the exception of the relaxation times, values for the various terms in equation (37) have been determined from a variety of physical measurements performed on graphite single crystals (50). The values of the corresponding electron and positive hole terms are very nearly the same in each case. The differences that do exist are such as to cause the electron terms to predominate. Therefore, if the analysis leading to equation (37) is substantially correct, three distinct attributes of the absolute thermoelectric power of graphite should be in evidence. It should be a linear function of the temperature, it should be small in absolute magnitude, and because the electronic charge e has an intrinsic negative sign it should be negative. These considerations are in excellent accord with the actual experimental observations of thermoelectric power measured between 300 and 725 °K, as will be seen in Section IV.

The linear relationship between thermoelectric power and temperature ceases to exist at somewhat lower temperatures (below 250° K) because of phonon drag (32,51) and, undoubtedly, at somewhat higher temperatures because of complete removal of degeneracy.

The sensitivity of the thermoelectric power to changes in the number of carriers produced by, for example, the chemisorption of a gas on the surface can be analyzed as follows: Let Δn be a small change in the number of negative carriers and let α_1 and α_2 be the values of thermoelectric power before and after this change. The fractional change of α is given by

$$\frac{\alpha_1 - \alpha_2}{\alpha_1} \simeq \frac{\Delta n\tau_e/m_e\mu}{n_e\tau_e/m_e\mu - n_p\tau_p/m_p(\Delta-\mu)}$$

$$\simeq \frac{\Delta n}{n_e - n_p\tau_p m_e\mu/\tau_e m_p(\Delta-\mu)} \qquad \text{(Eq. 38)}$$

Since for high purity graphite $n_e \simeq n_p$ (1), equation (38) can be written

$$\frac{\alpha_1 - \alpha_2}{\alpha_1} \simeq \frac{\Delta n}{n_e(1 - \xi)} \qquad \text{(Eq. 39)}$$

where $\xi \equiv \tau_p m_e \mu / \tau_e m_p (\Delta - \mu)$. The sensitivity is, therefore, high when: (*a*) $\xi \simeq 1$ and (*b*) n_e (and n_p) is relatively small (compared to metals, for example). Both of these conditions are fulfilled by high-purity graphite (see Section IV), so that sensitivity should be favorable to the investigation of chemisorption by means of changes in the thermoelectric power.

IV. Effect of Oxygen Chemisorption on Thermoelectric Power of Graphite

A. Description of Materials

The graphite employed in this study was a highly purified natural graphite having less than 6 ppm total impurity content and a specific BET surface area of 1.8 m^2/g (grade SP-1 from the Carbon Products Division of Union Carbide Corporation). From quantitative x-ray diffraction studies on the (0004) diffraction peak, using an internal standard (52), the interlayer spacing of the material was 3.3541Å at 15° C. Based on the Franklin (53) and Bacon (54) correlation, this indicates that the material has a minimum of stacking faults between the layer planes. Microscopic investigation revealed this powder to be composed of flake-like particles having a mean diameter of 30 microns on a number basis. A photograph showing this material enlarged by a factor of 100, along with a plot of the particle size distribution, is presented in Figure 6.1.

Particles were examined by direct transmission electron microscopy. As shown by Dawson and Follett (55,56), when the long axis of the particle runs parallel to the (000*l*) layer planes (as in the present case), crystallites in the particle are revealed by distinct and separate moiré patterns produced by gross stacking faults within individual crystallites. As expected from x-ray diffraction studies, the appearance of moiré patterns in the natural graphite was rarer than that found for artificial graphite by Dawson and Follett. Further, in most cases, there was no indication of the presence of microcrystallites composing the particles. Selected area electron diffraction studies produced, in most cases, single crystal patterns.

On the basis of these results it is concluded that the graphite particles are essentially nonporous. If it is assumed that the average particle may be

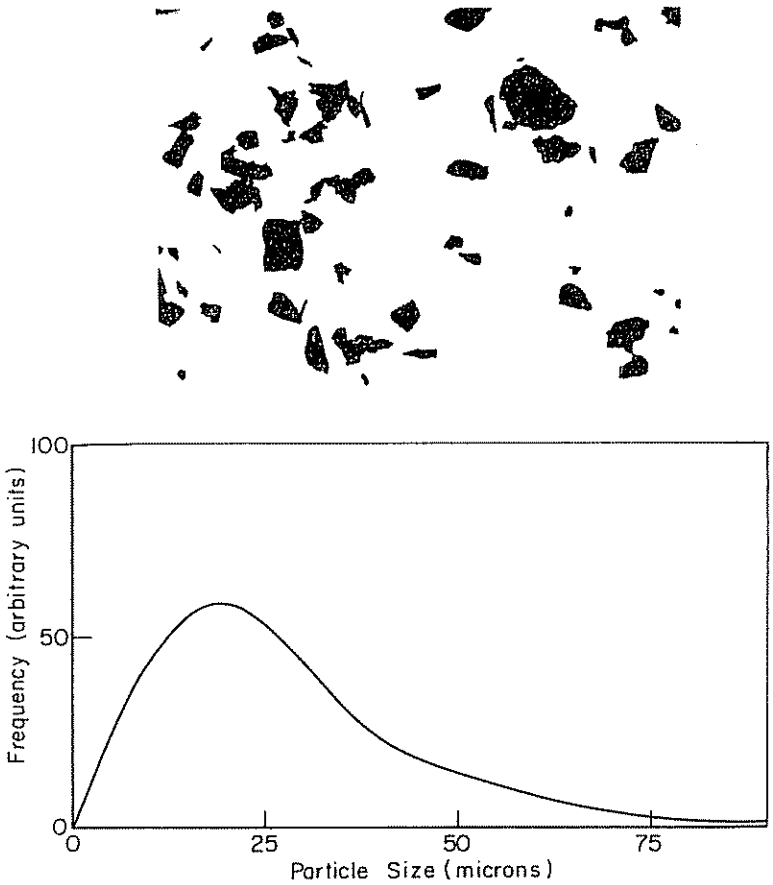

Figure 6.1. SP-1 Graphite flakes (× 100). SP-1 Graphite particle size distribution.

represented by a flat circular cylinder and that the reciprocal of the particle diameter is negligible in comparison with the reciprocal of the particle thickness, the surface area per unit weight is equal to twice the reciprocal of the product of the particle thickness and the particle density. Assuming that the particle density equals the crystallite density (2.269 g/cc) and taking the experimental value of 1.8 m^2/g for the specific surface area, the particle thickness is calculated to be 0.5 micron. By taking the top and bottom faces of the cylindrical graphite particles as being composed of basal planes [(000/) surface] and the circumference of the particles as being composed of prismatic planes ($10\bar{1}0$ and $11\bar{2}0$ surfaces), $10\bar{1}0$ and $11\bar{2}0$ planes are estimated to account for approximately 3.3 per cent of the total surface area of the particles.

In some cases iron (type SF iron powder from the General Aniline and Film Corporation) was added to the graphite, to study its effect on the kinetics of oxygen chemisorption. The iron, produced by the thermal decomposition of iron pentacarbonyl, was in the form of essentially spherical particles about 3 microns in diameter.

B. Sample Preparation

It has been shown previously that natural graphite can be compacted at room temperature to produce reasonably strong bodies (57). Details of sample preparation are given elsewhere (58). Briefly, rectangular bars were produced at a compaction pressure of 100,000 psi. The bars had the same BET surface area as the original graphite powder and an apparent density of 2.18 $\pm$ 0.03/g cc. From the apparent density of the bars and the x-ray density of the graphite particles, a porosity of 4 $\pm$ 2 per cent is calculated. Mercury porosimeter measurements revealed that this porosity existed almost exclusively in voids about 1000Å in diameter.

In order to both clean the surface of the graphite and anneal the sample to prevent any body expansion during thermoelectric power measurements, samples were heated slowly to 995° C and then soaked for one hour in a dry, oxygen-free helium atmosphere.

Samples were then prepared having different amounts of oxygen chemisorbed on their surfaces, by exposing them to a flowing oxygen stream at one atmosphere pressure at temperatures between 600 and 725° K. No detectable change in sample weight (certainly less than 0.025% weight change) was observed during the oxygen chemisorption, which indicates that a negligible quantity of graphite was gasified.

The amount of oxygen chemisorbed on the surface of the graphite was determined, after thermoelectric power measurements were made, in a modified version of the reactor-mass spectrometer complex employed by Walker and co-workers (7). The samples were outgassed at 950° C for three hours. The desorbed gases, consisting of carbon monoxide, carbon dioxide and hydrogen, were analyzed mass spectrometrically. A temperature of 950° C has been found sufficient to remove essentially all of the surface oxide, which is formed below 725° K, from graphite (8). It was found that the hydrogen was produced by the reaction of the graphite with residual water; that is, $C + H_2O \rightarrow H_2 + CO$. Therefore, the yield of total carbon monoxide was corrected for that resulting from the above reaction to give that produced only by complex decomposition. Each mole of carbon monoxide recovered from complex decomposition was taken as equivalent to one-half mole of molecular oxygen; each mole of carbon dioxide recovered was taken as equivalent to one mole of molecular oxygen.

C. *Thermoelectric Power Measurements*

The authors have investigated the effect of temperature and chemisorbed oxygen on the thermoelectric power of a highly purified, compacted, natural graphite and a corresponding system doped with a small amount of iron catalyst. For this purpose a thermoelectric power generator was constructed which allows the thermal emf to be measured, as a function of temperature, in either an inert or reacting atmosphere. A cross-sectional view of the principle component of this system is shown in Figure 6.2.

The generator is composed of a graphite-platinum couple in which the graphite element is molded in the form of a rectangular bar ($\frac{3}{8}$ in. × $\frac{3}{8}$ in. × 2 in.) with a $\frac{1}{8}$-in. diameter hole drilled through the center, parallel to the long axis of the block. The platinum element consists of two electrically insulated platinum plates incorporated in miniature furnace assemblies. The upper furnace is mobile and operates through a mechanism capable of applying a variable load to the furnace and sample. This provides a means of securing the graphite specimen between the two platinum plates at a fixed pressure and minimizes the effect of contact resistance variations arising from sample expansion during heating. The platinum plates are connected, by means of platinum wires, to a Rubicon High Precision, type B, potentiometer. The temperatures of the two junctions are measured by chromel-alumel thermocouples imbedded in the platinum plates. A sample encasement element is sealed to the mobile furnace and, after positioning of the graphite specimen between the platinum plates, is fastened to the stationary furnace by means of a carefully machined threaded ring and flanged coupling. This element isolates the graphite-platinum couple from the external atmosphere and permits the thermoelectric power measurements to be made in either an inert or reacting atmosphere. The sample encasement element incorporates stainless steel bellows which accommodate sample expansion during heating, and allows for slight variations in initial sample length. In addition, in order to avoid errors arising from large thermal gradients existing between this system and the laboratory atmosphere, the heated section of the apparatus is encased in a Transite housing which provides an air bath having a temperature close to the mean temperature of the thermoelectric junctions. In order to maintain the system as close to equilibrium as possible and still obtain significant voltages, the impressed thermal gradients were restricted to between 1 and 2° C/cm.

The thermoelectric power values obtained with this instrument were converted to absolute values by subtracting the contribution of the platinum reference. For this purpose the absolute thermoelectric power values of platinum were taken to be those reported by Borelius (59). In order to

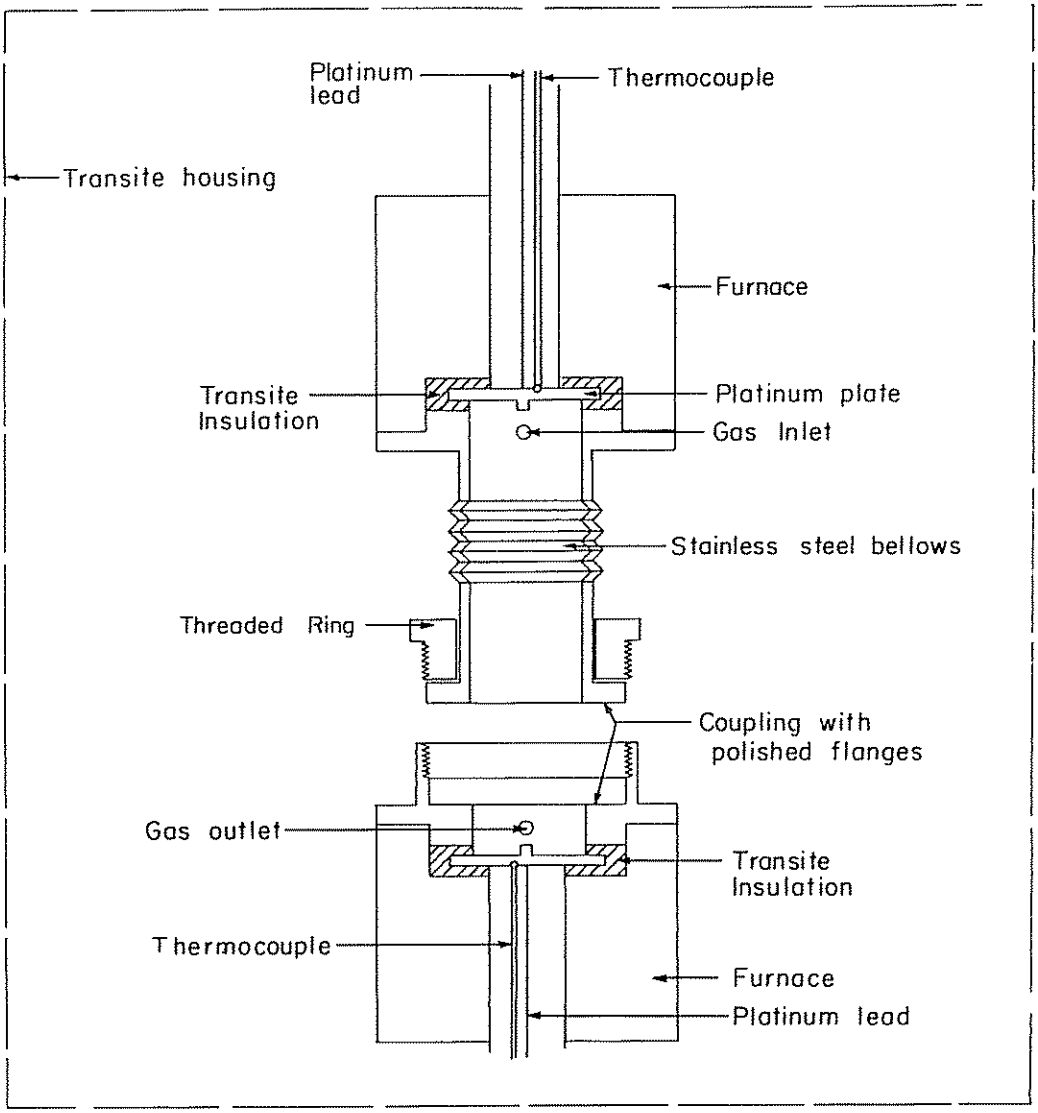

Figure 6.2. Thermoelectric generator.

check the accuracy of this instrument, measurements were made on chromel-P alloy (90 per cent Ni, 10 per cent Cr) over the temperature-range 300° K to 725° K. A temperature-independent value of $\alpha = 29.9 \pm 0.3\ \mu V/°K$ was obtained, which compares well with published values for this material of $\alpha = 30.3\ \mu V/°K$ (60).

D. Dependence of Thermoelectric Power of Graphite on Oxygen Chemisorption

When oxygen is chemisorbed on graphite, the thermoelectric power increases algebraically while maintaining its linear temperature dependence. This is shown in Figure 6.3 for different amounts of chemisorbed oxygen. It is noted that the degassed graphite had a measurable

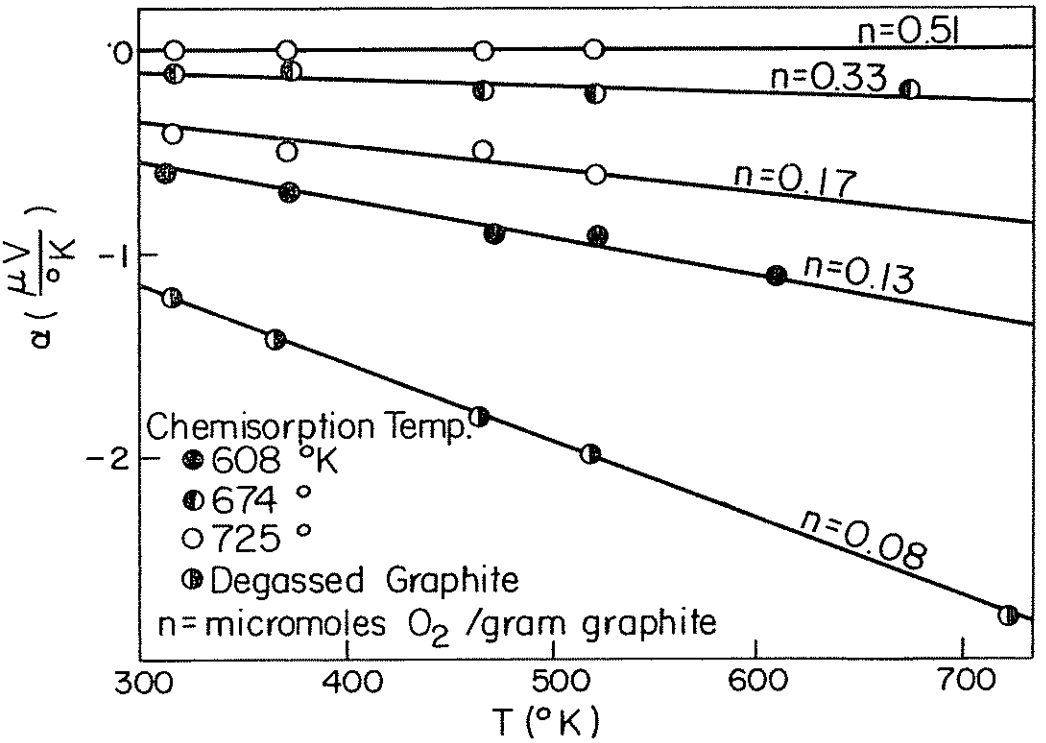

Figure 6.3. Temperature dependence of the thermoelectric power of SP-1 Graphite as a function of varying amounts of oxygen chemisorption.

amount of chemisorbed oxygen on its surface. It was not possible to maintain an oxygen-free graphite surface in equilibrium with air at room temperature. Between 0.07 and 0.08 micromole of oxygen per gram of graphite adsorbed on the specimen surface when the degassed samples (degassed either in helium at 995° C or *in vacuo* at 950° C) were exposed to the laboratory atmosphere at room temperature. A graphite surface containing this amount of adsorbed oxygen was found to be stable with respect to further room temperature air oxidation for a period of time as long as six months. It was confirmed that this oxide formation results

from exposure to air since additional oxide was not recovered when a degassed sample was cooled to room temperature *in vacuo* and then reheated to 950° C. Workers have found that some rapid chemisorption of oxygen on charcoal occurs at low temperatures. Keyes and Marshall (61) found that the heat of adsorption of oxygen at 0° C exceeded the latent heat of condensation sufficiently to ensure chemisorption. Later Bull, Hall, and Garner (62) found that at room temperature a charcoal powder chemisorbed quantitatively a charge of oxygen within 30 seconds, pointing to a very low activation energy. We will not be considering further in this review the process of rapid oxygen chemisorption at room temperature but rather the kinetics of oxygen chemisorption which occurs at high temperatures and has a sizeable activation energy.

The algebraic increase in the thermoelectric power values with increase in amount of oxygen chemisorbed on the surface is readily understood in terms of equation (37), if it is assumed that the chemisorbed oxygen localizes p_z electrons in surface states. This would simultaneously reduce the number of electrons and increase the number of positive holes, causing the thermoelectric power to increase algebraically. The totally unexpected case of oxygen donating electrons to the conduction system would have the reverse effect. Another alternative would be to assume that the surface oxide acts as an additional scattering center. However, since the positive holes are in general of lower energy than the negative carriers, additional scattering centers should be more effective in limiting the mobility of the positive holes. This would reduce the contribution of the positive hole terms relative to the electron terms and cause the thermoelectric power to become more negative, which is not in agreement with the experimental observations.

Qualitatively, the conclusion that oxygen chemisorption localizes p_z electrons in surface states is supported by limited data on the heat of chemisorption of oxygen on carbon. The heat of chemisorption is *ca.* 100 kcal/mole of oxygen (62). In the most straightforward way, the heat of chemisorption can be estimated from bond energy data for the C=O and O=O bonds, that is, $q = 2E_{(C=O)} - E_{(O=O)}$. Taking $E_{(C=O)} = 175$ kcal (63) and $E_{(O=O)} = 118$ kcal (64), $q = 232$ kcal/mole of oxygen. This figure is much higher than the experimental heat of chemisorption. However, a simple model suggests itself for the type of carbon-oxygen bond that might account for the localization of p_z electrons in surface states upon oxygen chemisorption. The surface complex may involve a carbonyl structure in which a σ bond is formed by the overlap of an oxygen p_x orbital with an edge carbon sp^2 hybrid orbital and a π bond is formed from the overlap of the oxygen and carbon p_z orbitals.

Considering this to effectively reduce a C=C bond to a C—C bond, a

decrease of $2(E_{(C=C)} - E_{(C-C)})$ in the above calculated heat should be made. Taking $E_{(C=C)} = 140$ kcal and $E_{(C-C)} = 80$ kcal (63), the heat of chemisorption is 112 kcal/mole, which is in reasonable agreement with experiment. The results of this calculation do not necessarily lead to the conclusion that the formation of each oxygen complex completely localizes one p_z electron. If, on the average, only partial localization occurs, the energy of the bond between carbon and oxygen in the complex will be less than 175 kcal; but also a C=C bond will not, on the average, be decreased all the way to a C—C bond. These effects will compensate each other, producing about the same calculated heat of chemisorption as previously given.

The dependence of the thermoelectric power on the extent of surface oxidation, at a specific temperature, may be obtained from the data of Figure 6.3. This is shown in Figure 6.4 at a temperature of 720° K. The general shape of this curve is consistent with equation (37), if it is assumed that the change in the number of current carriers is a linear function of the amount of chemisorbed oxygen and account is taken of the dependence of the Fermi energy on the current carrier density. That is, if the terms β_e and β_p are defined so as to measure the position of the Fermi energy from the bottom of the conduction band and the top of the valence band, respectively, then

$$\beta_e = \mu \qquad \text{(Eq. 40)}$$

and

$$\beta_p = \Delta - \mu \qquad \text{(Eq. 41)}$$

since the bottom of the conduction band has been taken as the zero of energy. Then, if the temperature dependence of the Fermi energy is considered negligible, we may write (65)

$$\beta_i = \frac{h^2}{2m_i}\left(\frac{3n_i}{8\pi}\right)^{2/3} \qquad i = e, p \qquad \text{(Eq. 42)}$$

Therefore, if the denominator of equation (37) remains essentially constant as n_p increases and n_e decreases, a fractional order dependence of α on n should be expected, with the order being approximately $\frac{1}{3}$.

For small amounts of oxygen chemisorbed on the graphite, the thermoelectric power is very sensitive to the amount adsorbed. Undoubtedly, this is responsible at least for part of the wide range of thermoelectric power values reported in the literature for supposedly high-purity graphite.

It is of interest to estimate the thermoelectric power of high-purity graphite using equation (37). Since the mobility of the carriers equals

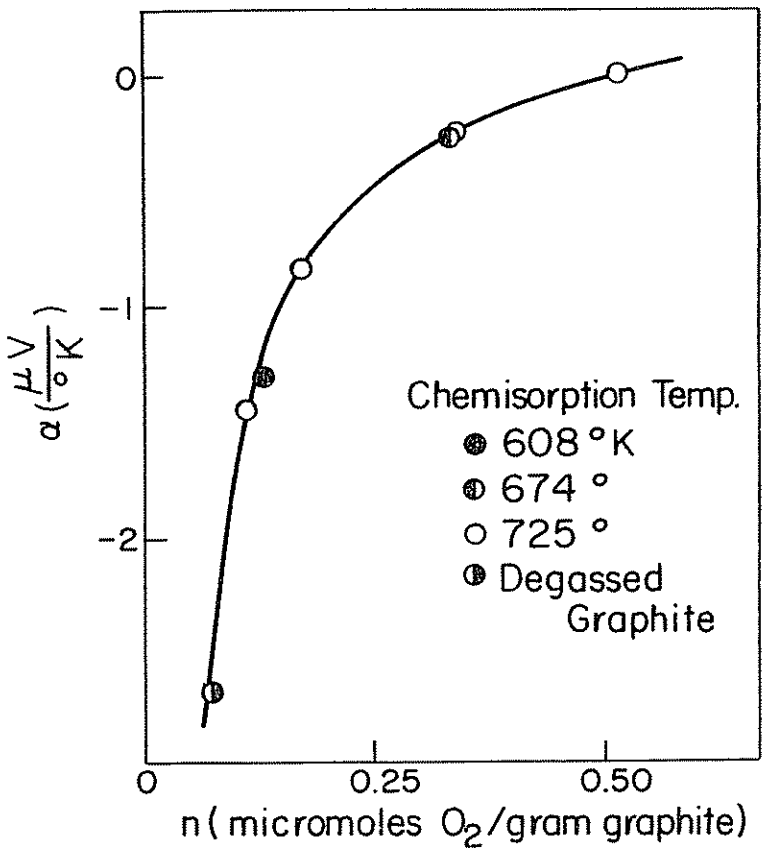

Figure 6.4. Dependence of the thermoelectric power of SP-1 Graphite at 720° K on the amount of chemisorbed oxygen.

$e\tau_i/m_i$, if we let the ratio of electron-to-hole mobility equal b and the ratio of the number of positive carriers to negative carriers equal a, equation (37) becomes

$$\alpha = \frac{\pi^2 k_B^2 T}{2e}\left[\frac{b/\mu - a/(\Delta - \mu)}{a + b}\right] \qquad \text{(Eq. 43)}$$

or

$$\alpha = -3.7 \times 10^{-2} T\left[\frac{b/\mu - a/(\Delta - \mu)}{a + b}\right] \qquad \text{(Eq. 44)}$$

in μV/°K, where μ and $(\Delta - \mu)$ are in eV. The calculated thermoelectric power is extremely sensitive to the values selected for the parameters a, b, μ, and $(\Delta - \mu)$. There appears to be rather general agreement that a

is about 1.0 and, at 300° K, b is about 1.1 (1). Soule suggests a value of 0.018 eV for μ (50). To obtain the experimental value for α at 300° K (that is, $-1.2\ \mu V/°K$), $(\Delta - \mu)$ will equal 0.0165 eV. This value appears reasonable since Soule suggests that Δ is about 0.035 eV and that, for pure graphite, the Fermi level lies approximately in the middle of the band overlap region (66).

In fact, the graphite used in this study may have had some oxygen still chemisorbed on its surface following degassing at 995° C. This suspicion is based on the following facts: (*1*) Recently, in this laboratory, the thermoelectric power of an extruded spectroscopic graphite electrode (filler plus binder) has been measured along its extrusion direction as $-2.0\ \mu V/°K$ at 300° K. This electrode did not have as high a degree of preferred particle (or crystallite) alignment as the molded natural graphite samples used in this study; and, therefore, this lower value cannot be attributed to a lower c-axis participation in the α value. (*2*) Results on degassing spectroscopic graphite (67) show that carbon monoxide can be recovered at least up to 1600° C. (*3*) Blackman, Dundas, and Ubbelohde (31) found the thermoelectric power of pyrolytic graphite in the a-axis direction to be as high as $-11.2\ \mu V/°K$ at room temperature.

Unfortunately, as was shown recently (68), natural graphite pellets progressively decrease in strength with increasing degassing temperatures. It would have been difficult to handle much weaker pellets during measurements in our thermoelectric power apparatus.

Only a slight decrease in the carrier concentration ratio in equation (44) would yield a calculated α of $-11.2\ \mu V/°K$. This agrees with the previous conclusion, based on Figure 6.4, that α changes very markedly with carrier concentration when the active carbon surface is only sparsely covered with complex.

V. Kinetics of Oxygen Chemisorption on Graphite

A. Experimental Results for Rate of Oxygen Chemisorption

The rate of oxygen chemisorption on graphite may be determined as a result of the correlation between α and n. This is accomplished by following the change in the thermoelectric power, at a specific temperature, during the process of oxygen chemisorption and converting the thermoelectric power values to amounts of chemisorbed oxygen. Data obtained in this manner, for different samples of pure graphite at three specific temperatures, are presented in Figure 6.5. The circles represent the actual experimental values while the curves have been calculated as a result of the following analysis.

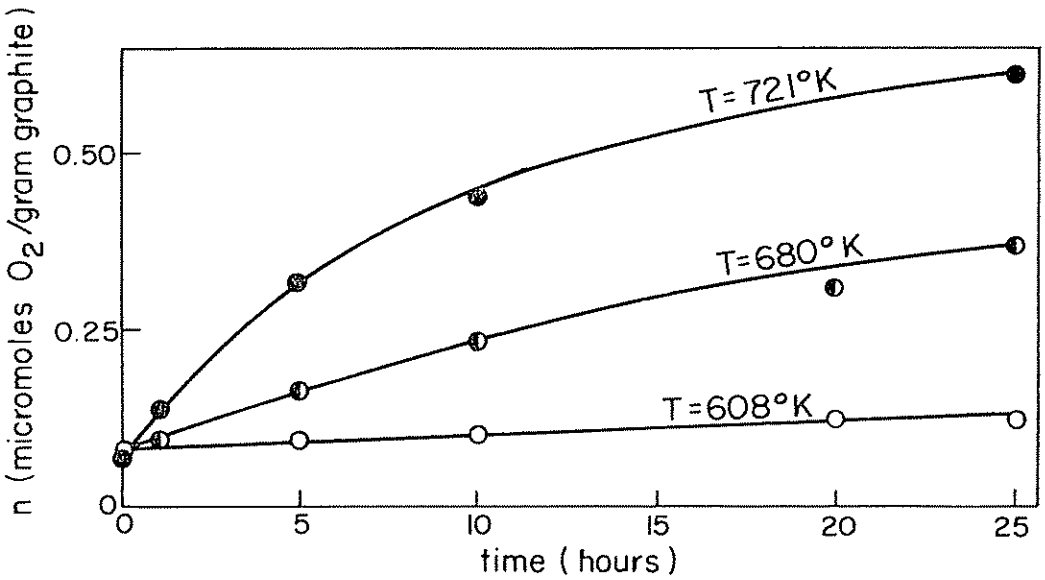

Figure 6.5. Rate of oxygen chemisorption on SP-1 Graphite.

If it is assumed that the velocity of chemisorption is first order with respect to both reactants, the rate equation may be expressed as

$$\frac{dn'}{dt'} = kC(1 - \theta)n_\infty \qquad \text{(Eq. 45)}$$

where n' is the amount of oxygen chemisorbed on the graphite surface at time t', k is the rate constant, C is the concentration of oxygen in the gas phase, θ is the fraction of the active surface area covered at time t', and n_∞ represents the saturation amount of chemisorbed oxygen. In terms of these variables

$$\theta = \frac{n'}{n_\infty} \qquad \text{(Eq. 46)}$$

Substituting this expression for θ and integrating equation (45) between the limits of $n' = n_0$ at $t' = 0$ and $n' = n$ at $t' = t$ yields

$$n = n_\infty - (n_\infty - n_0) \exp(-kCt) \qquad \text{(Eq. 47)}$$

Curves calculated from equation (47) were fitted to the experimental data by adjusting the values of n_0, n_∞, and k. The values of n_0 selected for this calculation were determined experimentally. This had the effect of reducing

the trial fitting to a two parameter problem. The values of n_0, n_∞, and k used to obtain the type of fit shown in Figure 6.5 are presented in Table 6.1.

Table 6.1. Kinetic Parameters for Oxygen Chemisorption on SP-1 Graphite

T °K	n_0 μM/g	n_∞ μM/g	k cc/mole-sec
608	0.08	0.66	0.046
608	0.10	0.68	0.053
674	0.09	0.64	0.49
680	0.08	0.64	0.46
721	0.07	0.62	2.04

The values of n_∞ required for these calculations are approximately the same for each graphite specimen and show no apparent temperature dependence. This first observation may be taken as an indication of a high degree of sample reproducibility, while the latter demonstrates the essentially irreversible nature of oxygen chemisorption on graphite at temperatures below 721° K. The constancy of the n_∞ values with respect to temperature is a necessary condition for the analysis to be self-consistent since it is tacitly assumed in formulating equation (45) that the rates of desorption processes are negligible. The total active surface area may be calculated from the n_∞ values if it is assumed that the chemisorption process occurs primarily on edge carbon atoms. These atoms, which lie in the $10\bar{1}0$ and/or $11\bar{2}0$ planes, have an effective area of about 8.3 Å^2. The result of such a calculation for a value of n_∞ equal to 0.65 yields a total active surface area which accounts for 3.7 per cent of the total BET surface area.

It was previously calculated, from the dimensions of the graphite particles, that *ca.* 3.3 per cent of the particle surface is composed of $10\bar{1}0$ and/or $11\bar{2}0$ planes. The close agreement between this figure and that for the percentage of particle surface capable of forming a surface oxygen complex leads to the conclusion that the basal-plane surface of graphite is essentially inactive to the chemisorption of oxygen. This conclusion is in conflict with that of Savage (69), who studied the chemisorption of oxygen on graphite wear dust somewhat above room temperature. Savage found that oxygen adsorbed on about 25 per cent of the wear-dust surface, a figure he concluded to be considerably in excess of the percentage of edge surface present in the particles. There may be at least three reasons for this discrepancy: (*1*) Oxygen can probably chemisorb at dislocations in the basal plane; the severe mechanical treatment of the graphite, resulting in particle breakage to produce wear dust, would be expected to result in a

very high dislocation density. (*2*) Particle breakage was performed in an oxygen atmosphere; chemisorption could have taken place on the freshly exposed surface before annealing of the more unstable defects occurred. (*3*) There was possible oxidation of the fresh impurity metal surface produced concurrently with the graphite wear dust; that is, the wear dust was formed by rubbing graphite rods against a spinning copper ring.

It is of considerable interest to note that it was not necessary to assume a dependence of the rate constants on the extent of surface coverage in order to account for the experimental results. This implies that the activation energy for this reaction does not vary significantly with the amount of surface complex formed. However, the energy requirements for surface complex formation should increase as the amount of complex increases, since it was concluded that the process of oxygen chemisorption on the graphite surface removes current carriers from the conduction system. Then, as the Fermi energy recedes from the Brillouin zone boundary, an increase is necessitated in the amount of energy required to promote an electron from the conduction system into a surface state. Therefore, if the energy of the activated complex for the reaction decreases less than the Fermi energy, one would expect an increase in the amount of surface oxide formed to result in an increase in the activation energy. While this mechanism follows quite naturally from the preceding discussions and may be of considerable importance with regard to the general problem of activation energy variation during chemisorption, it must necessarily be of only minor significance to the reaction under consideration. Even if the chemisorbed oxygen achieved the improbable efficiency of removing one electron from the conduction system per oxygen atom, the n_∞ values dictate that a limit of the order of 10^{18} current carriers per unit volume would be localized in surface states. It then follows from equation (42), using an average value of $0.05m_0$ for the effective mass (50) (m_0 is the mass of a free electron), that the Fermi energy recession would be limited to the order of 0.01 electron volt (*ca.* 200 calories). The accompanying change in the activation energy would then be too small to be observed experimentally. These considerations suggest a possible means of checking the credibility of the proposed mechanism for activation energy variation during sorption processes. A sufficient quantity of surface complex might be formed to produce a measurable change in the activation energy if the active surface area per unit volume was increased by a factor of several hundred. The increase in the active surface area might be obtained by grinding the graphite flakes prior to their purification.

The thermoelectric power, measured as a function of temperature, of degassed graphite containing 0.3 per cent iron and maintained in a helium atmosphere was found to be precisely the same as that of the pure graphite

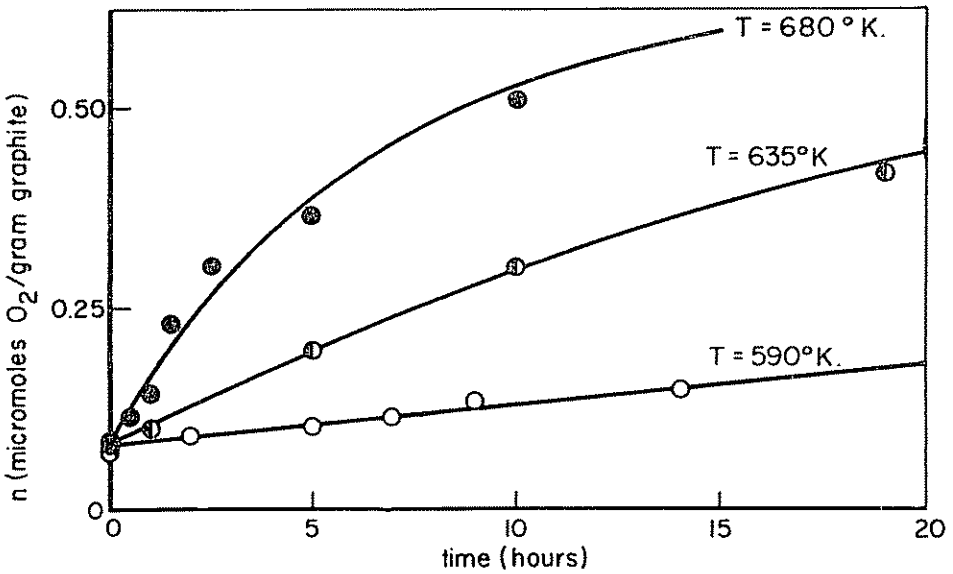

Figure 6.6. Rate of oxygen chemisorption on SP-1 Graphite doped with 0.3% iron.

when measured under the same conditions. However, when the chemisorption experiment was repeated with this material, the reaction rates, at a given temperature, were observed to be higher than in the case of the pure graphite. The catalytic activity of the iron is considered to be a localized effect because of the absence of evidence for an electronic interaction between the iron and graphite. The kinetics of this reaction were found to be explicable in terms of the same analysis used for the pure material. Representative data along with the calculated curves are shown in Figure 6.6. A complete list of the values of n_0, n_∞, and k for the different chemisorption temperatures is presented in Table 6.2. No significant change in n_0 or n_∞ resulted from the addition of iron to the graphite.

In order to insure the consistency of the kinetic analysis and to summarize the comparison of the catalyzed and uncatalyzed reactions,

Table 6.2. Kinetic Parameters for Oxygen Chemisorption on SP-1 Graphite Containing 0.3 Per Cent Iron

° K	n_0 μM/g	n_∞ μM/g	k cc/mole sec
590	0.08	0.68	0.12
608	0.09	0.67	0.21
635	0.08	0.71	0.62
680	0.09	0.65	2.32

Arrhenius plots were prepared and appear in Figure 6.7. The activation energies and preexponential term values are included in this figure.

Although the calculated activation energy is lower in the case of the iron-graphite system, it is not certain that this accounts for the catalytic activity of the iron. There is sufficient scatter in the data to introduce an uncertainty in the activation energy values of ± 2 kcal/mole. It is doubtful that an increase in the number of experimental observations would improve this situation. The system incorporates a thermal gradient which fluctuates slightly in magnitude during the course of a run. Therefore, the reaction velocity for a given experiment represents an average over a

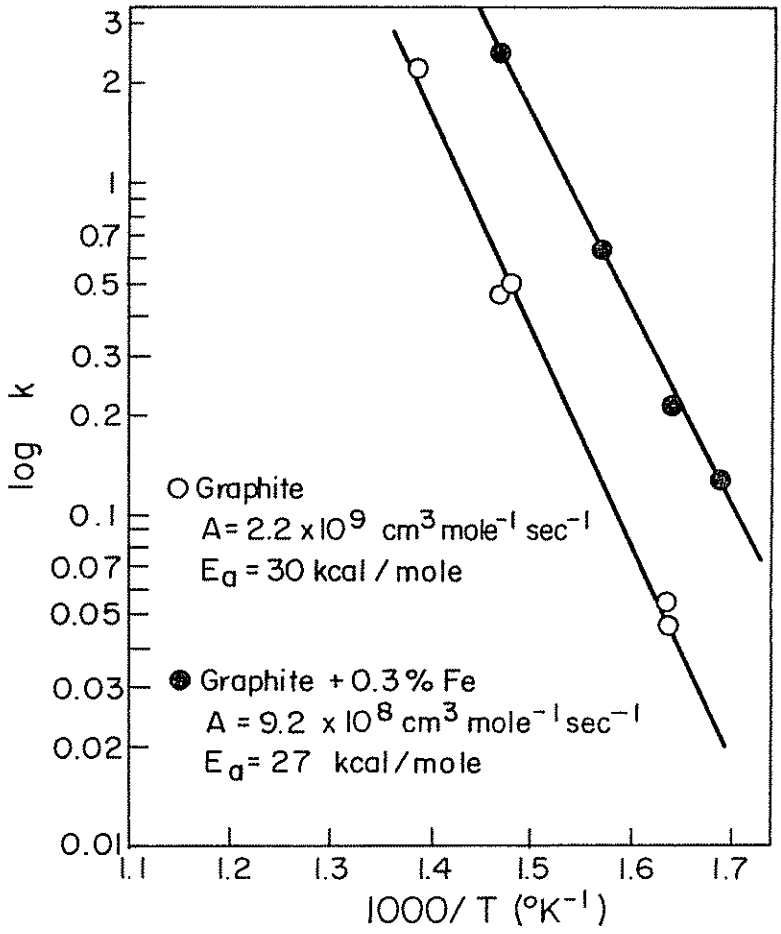

Figure 6.7. Arrhenius plots for the catalyzed and uncatalyzed chemisorption of oxygen on SP-1 Graphite.

small temperature interval. This departure from isothermal conditions introduces an intrinsic error which prevents an accurate evaluation of the temperature dependence of the rate constants.

B. The Nature of the Activated Complex Leading to Chemisorption

The rate equation used to fit the experimental results is given by equation (45). The rate constant of activated chemisorption k can be expressed in terms of an entropy and an enthalpy of activation by using absolute rate theory concepts (70). Let $\theta^{\ddagger}$ be the fractional coverage of the reacting surface by an activated transition complex of $C(O_2)^{\ddagger}$. This activated state can decay back to a bare active surface site and free oxygen, or it can transform to oxygen chemisorbed on the surface. Rate equation (45) is an irreversible form; therefore, the nature of the chemisorbed oxygen and the heat of adsorption is of no concern to the rate equation. Because of the high activation energy for formation of the transition complex, it can be assumed that it is in equilibrium with bare sites and free oxygen, so that

$$K^*(C/C_0)(1 - \theta)n_\infty = \theta^{\ddagger}n_\infty \qquad \text{(Eq. 48)}$$

K^* is the equilibrium constant of formation of the activated complex, C_0 is the standard state chosen for gas concentration. The rate of reaction to form adsorbed oxygen is, in the usual way

$$dn/dt = (\text{frequency of transition})\theta^{\ddagger}n_\infty \qquad \text{(Eq. 49)}$$

Replacing $\theta^{\ddagger}$ from equation (48), and performing the usual manipulations, gives

$$dn/dt = (k_BT/h)(C/C_0)(1 - \theta)K^{\ddagger}n_\infty \qquad \text{(Eq. 50)}$$

$K^{\ddagger}$ is the truncated equilibrium constant obtained from K^* by the removal of the partition function of the weak decay vibration. Equation (50) can be put in the form

$$dn/dt = k'(C/C_0)(1 - \theta)n_\infty \qquad \text{(Eq. 51)}$$

By comparing equation (51) with equation (45), we show that the experimental value of k (which has the units of cc mole^{-1} sec^{-1}) is related to the thermodynamic rate constant k' (which has units of sec^{-1}) by $k' = kC_0$. The magnitude of the entropy of activation depends on the standard state chosen for C_0. From the usual treatment according to absolute rate theory,

$$k' = (k_BT/h)\exp(\Delta S_T^{0\ddagger}/R)\exp(-\Delta H_T^{0\ddagger}/RT) \qquad \text{(Eq. 52)}$$

A Φ-value can be defined by

$$\Phi = S^0_T - (H^0_T - H^0_0)/T \qquad \text{(Eq. 53)}$$

Then

$$k' = (k_B T/h) \exp(\Delta\Phi^{\ddagger}/R) \exp(-\Delta H^{0\ddagger}_0/RT) \qquad \text{(Eq. 54)}$$

In equation (54) $\Delta H^{0\ddagger}_0$ is the zero point enthalpy of activation. When comparing equation (54) with the Arrhenius equation, $k' = A\exp(-E/RT)$, it is common practice to equate E with ΔH^0_0 and A with

$$(k_B T/h) \exp(\Delta\Phi^{\ddagger}/R)$$

Following this practice and converting to a standard state of one atmosphere, the values of $\Delta\Phi^{\ddagger}$ calculated from the experimental data reported in Section IV are about -38.5 cal/° K gm mole O_2 (eu) for oxygen chemisorption on the high-purity graphite surface and about -40.5 eu for oxygen chemisorption on the graphite containing 0.3% iron.

The loss in entropy for mobile or immobile adsorption can be calculated as described by Trapnell (72). The formulas used are

$$ {}_3S^0_{\text{trans}} = R \ln (M^{3/2} T^{5/2}) - 2.30 \qquad \text{(Eq. 55)}$$

$$ {}_2S^0_{\text{trans}} = R \ln (MTA) + 65.80 \qquad \text{(Eq. 56)}$$

${}_3S^0_{\text{trans}}$ is the translational entropy, at a standard state of one atmosphere, of the three translational degrees of freedom of the free gas molecule of molecular weight M. ${}_2S^0_{\text{trans}}$ is the two-dimensional entropy of translation of the mobile transition complex, each complex possessing two degrees of translational freedom within an area A occupied by a carbon site (or carbon sites). The minimum possible value ${}_2S^0_{\text{trans}}$ (which we shall see is of interest to us in our calculations) is given when the complex is assumed to be in translation around a single site. A equals *ca.* 8.3Å² for edge carbon sites in the $10\bar{1}0$ and $11\bar{2}0$ planes.

The rotational entropy of the free gas oxygen molecule is given by Glasstone (73) as

$$S^0_{\text{rot}} = R(\ln I + \ln T + 88.59) \qquad \text{(Eq. 57)}$$

where I is the moment of inertia of the molecule. [The value of $\Delta\Phi^{\ddagger}$ obtained experimentally is a differential change based on the Langmuir isotherm. Therefore, we are not concerned with the absolute entropy of the surface transition complex, but the differential change in entropy.

The differential change in configurational entropy for fixed site adsorption, according to a Langmuir isotherm, reduces to the θ, $(1 - \theta)$ terms which have already been included in the analysis leading to equation (54). Therefore, there is no need to calculate configurational entropies.]

The values obtained from applying these formulas at $T = 650°$ K are ${}_3S^0_{\text{trans}} = 40$ eu, ${}_2S^0_{\text{trans}} = 17$ eu, and $S^0_{\text{rot}} = 12$ eu. Thus, if the activated complex were mobile and lost no rotational entropy, $\Delta S^\ddagger$ would have a maximum value of -23 eu (neglecting vibrational terms); if it were mobile and lost all the rotational entropy, $\Delta S^\ddagger$ would have a maximum value of -35 eu. Neither of these cases gives sufficient entropy change to explain the experimental value of $\Delta\Phi^\ddagger$. Further, there is no reason to expect that all of the rotational entropy would be lost. Therefore, it seems likely that the activated complex is an immobile complex.

From the definition of Φ, the $\Delta\Phi$ of activation can be expressed as

$$\Delta\Phi^\ddagger = \Delta S^0_T - (\Delta H^0_T - \Delta H^0_0)/T \qquad \text{(Eq. 58)}$$

The entropy values do not have linear temperature dependencies, but the value of ΔH^0_T does. As a first approximation, we can express $(\Delta H^0_T - \Delta H^0_0)$ as

$$\Delta H^0_T - \Delta H^0_0 = 2RT - (2.5RT + RT) \qquad \text{(Eq. 59)}$$

The first term on the right hand side of equation (59) assumes that the heat capacity of the immobile complex can be approximated by $\frac{2}{3}$ the heat capacity of an ideal solid (maximum value to be expected), while the second term is the heat capacity term for oxygen. Substituting in equation (58) gives

$$\Delta\Phi^\ddagger = \Delta S^0_T + \tfrac{3}{2}R = \Delta S^0_T + 3 \text{ eu} \qquad \text{(Eq. 60)}$$

It is, therefore, valid to compare the experimental $\Delta\Phi^\ddagger$ values with calculated standard state entropy values, since the difference between the two is not large.

The most reasonable explanation of the state of the activated complex is that it has lost all three translational degrees of freedom (-40 eu) and has probably lost some of one degree of rotational freedom. The freedom corresponding to spin around the axis between the oxygen atoms is probably retained, but there is likely to be hindered rotation in the other degree of rotational freedom. On the other hand, the activated complex will gain some vibrational freedom terms, although these will be relatively small. Assuming that the partial loss of rotational freedom is counterbalanced by the gain of vibrational freedoms, the model would predict a $\Delta\Phi^\ddagger$ of $-40 + 3$ (equation 60) or about -37 eu. This agrees well with the

experimental results. (It must be remembered that the activation energies are uncertain to the extent of about ± 2 kcal/mole; this leads to an uncertainty in the entropy values of about ± 3 eu.)

To the authors' knowledge, no theoretical estimate has yet been made of the activation energy of oxygen chemisorption on graphite. For simple assemblies of atoms at known distances apart, the total energy may be calculated from the forces between the atoms. Consequently, for a simple system it is possible to calculate the change in energy as the molecules approach each other from infinity and interact chemically. The maximum extent to which intermediate configurations possess a greater energy than that of the separated reactants is the activation energy. Using this approach, the activation energy for hydrogen chemisorption on carbon has been calculated by Sherman and Eyring (74). The authors showed that the activation energy should be very sensitive to the distance between the carbon atoms, on which eventually the two hydrogen atoms chemisorb. At very high separations of the carbon atoms, the molecule must effectively be dissociated prior to adsorption. The activation energy would be high and approach the heat of dissociation of the molecule. At very low separations of the carbon atoms, the activation energy is again high because adsorption is hindered by repulsion forces. Sherman and Eyring find that the minimum activation energy for dissociative hydrogen chemisorption occurs when the distance between the carbon atoms is 3.5 Å. It is noteworthy that this is very close to the spacing between basal planes in graphite and, consequently, carbon atoms in adjacent planes.

In the case of oxygen chemisorption, where the complex formed goes to carbon monoxide upon desorption, it is expected that the activated complex for adsorption involves two adjacent surface carbon atoms. The prevalent distances between edge surface carbon atoms are 3.35 Å for atoms in two adjacent basal planes, 2.46 Å for atoms in a basal plane along the $\langle 11\bar{2}0 \rangle$ direction, 1.42 Å and 2.84 Å for atoms in a basal plane along the $\langle 10\bar{1}0 \rangle$ direction. It would be of interest to see if a theoretical activation energy versus carbon-carbon distance plot favors one of these four spacings for the formation of the activated complex.

VI. Summary

The thermoelectric power of a highly purified, compacted, natural graphite was measured over the temperature interval 300° K to 725° K. The experimental results are consistent with an analysis, based on the general theory of transport phenomena in solids, which assumes cylindrical constant energy contours near the Brillouin zone corners, an energy-independent relaxation time approximation for conduction electron

scattering, and only slight thermal broadening of the distribution function at the Fermi surface.

It was observed that chemisorption of oxygen on the graphite surface caused the thermoelectric power to increase algebraically while maintaining a linear temperature dependence. It is concluded that this effect is caused by the removal of p_z electrons from the conduction system in the formation of the surface complex. This explanation is substantiated both by the direction of the change and the general functional dependence of the thermoelectric power on the amount of chemisorbed oxygen.

It has been demonstrated that thermoelectric power measurements may be used to determine the rate of oxygen chemisorption on high purity graphite and graphite to which 0.3% iron was added. The general conclusions that followed from this investigation are as follows:

1. The reaction is first order with respect to both the active graphite surface and the oxygen concentration in the gas phase.

2. The total active surface area represents approximately 4% of the total BET surface area. This suggests that the reaction is confined to the edge atoms of the crystallite planes.

3. The rate constant is independent of the extent of surface coverage.

4. The values of entropy of activation indicate that the activated complex of chemisorption is an immobile complex.

5. Iron is an active catalyst for the chemisorption of oxygen on graphite. Although little reliable information was obtained with regard to the mechanism of this catalysis, the absence of any evidence for an electronic interaction between the iron and graphite suggests that the catalytic process is a localized phenomenon.

Acknowledgments

We wish to express our appreciation to the U.S. Atomic Energy Commission for support of our studies on gas-carbon reactions. Their support through Contract No. AT(30-1)-1710 made this contribution possible. We appreciate the constructive comments of P. Grosewald.

Nomenclature

A	Preexponential factor in equation, $k' = A \exp(-E/RT)$
a	Ratio of n_p to n_e
b	Ratio of electron to positive hole mobility
C	Concentration of oxygen in the gas phase
C_0	Standard state chosen for gas concentration

$\Delta H_T^{0\ddagger}$	Standard state enthalpy of activation at temperature T
$\Delta S^{\ddagger}$	Calculated standard state entropy of activation at $T = 650°$ K
$\Delta S_T^{0\ddagger}$	Standard state entropy of activation at temperature T
e	Electronic charge
$\mathscr{E}$	Electrical field
E	Activation energy or electron energy
f	Non-equilibrium distribution function
f_0	Equilibrium distribution function
H_0^0	Standard state enthalpy at absolute zero
H_T^0	Standard state enthalpy at temperature T
h	Planck's constant
$\hbar$	Planck's constant divided by 2π
I	Moment of inertia of molecule
$\mathbf{J}$	Electrical current per unit volume
k	Rate constant for oxygen chemisorption
k'	$(k_B T/h)K^{\ddagger}$
k_B	Boltzmann constant
$K^{\ddagger}$	Truncated equilibrium constant, i.e., the partition function of the weak decay vibration is factored from K^* to leave $K^{\ddagger}$
K^*	Equilibrium constant of formation of activated complex
$\mathbf{K}$	Momentum or wave vector
m_e	Effective mass of electrons
m_0	Mass of a free electron
m_p	Effective mass of positive holes
M	Molecular weight
n	Amount of oxygen chemisorbed on graphite at time t
n_α	Amount of oxygen chemisorbed on graphite at $t = \alpha$
n_e	Number of electron carriers
n_0	Amount of oxygen chemisorbed on graphite at $t = 0$
n_p	number of positive hole carriers
P_m	Molding pressure
$\mathbf{Q}$	Thermal flux per unit volume
$\mathbf{r}$	Position vector
S	Area
S_T^0	Standard state entropy at temperature T
t	Time
$\mathbf{v}$	Electron velocity
α	Thermoelectric power
Δ	Overlap of valence and conduction bond
$\Delta\Phi^{\ddagger}$	See Equation 58
μ	Fermi energy
τ	Characteristic relaxation time

θ Fraction of active surface of graphite covered by chemisorbed oxygen

$\theta^{\ddagger}$ Fractional coverage of the reacting surface by an activated transition complex of $(CO_2)^{\ddagger}$

Φ See equation 53

References

1. Ubbelohde, A. R., and F. A. Lewis, *Graphite and Its Crystal Compounds*, Clarendon Press, Oxford, 1960, pp. 68–108.
2. Nightingale, R. E., H. H. Yoshikawa, and H. H. W. Losty, in R. E. Nightingale, ed., *Nuclear Graphite*, Academic Press Inc., New York, 1962, pp. 132–144.
3. Blackman, L. C. F., *Research (London)*, **13,** 441 (1960).
4. Klein, C. A. *Rev. Modern Phys.*, **34,** 56 (1962).
5. Smith, R. Nelson, *Quart. Rev. (London)*, **13,** 287 (1959).
6. Culver, R. V., and H. Watts, Rev. Pure Appl. Chem., **10,** No. 2, 95 (1960).
7. Laine, N. R., F. J. Vastola, and P. L. Walker, Jr., *Proc. Conf. Carbon, 5th, Penn. State Univ., 1961*, Vol. **2,** 211 (1962).
8. Laine, N. R., F. J. Vastola, and P. L. Walker, Jr., *J. Phys. Chem.*, **67,** 2030 (1963).
9. Savage, R. H., and C. Brown, *J. Am. Chem. Soc.*, **70,** 2362 (1948).
10. Walker, P. L., Jr., and S. B. Seeley, *Proc. Conf. Carbon, 3rd, Buffalo, 1957*, 481 (1959).
11. Savage, R. H., *J. Appl. Phys.*, **19,** 1 (1948).
12. Zettlemoyer, A. C., N. Tcheurehdjian, and C. L. Hosler, *J. Appl. Math. and Phys.*, **14,** 496 (1963).
13. Mrozowski, S., United States Patent 2,682,686 (1954).
14. Zelinski, J. J., Ph.D. thesis, The Pennsylvania State University, 1950.
15. Graham, D., *J. Phys. Chem.*, **59,** 896 (1955).
16. Smith, W. R., *Encyclopedia of Chemical Technology*, Vol. 3, Interscience Publishers, New York, 1949, pp. 61–62.
17. Nightingale, R. E., *Nuclear Graphite*, Academic Press, New York, 1962, pp. 1–17.
18. Palme, A., *Elektrotechn. Z.* **23,** 413 (1905).
19. Iljev, A. M., *Jurn. Russk. Fisik.-Chimicesk. Obscestva* **40,** 220 (1908).
20. van Aubel, E., *Compt. Rend.* **153,** 568 (1911).
21. Bidwell, C. C., *Phys. Rev.*, **3,** Ser. 2, 450 (1914).
22. Gottstein, G., Ann. Physik, **43,** 1079 (1914).
23. LaRosa, M., *Nuovo Cimento*, **12,** 284 (1916).
24. Hukuda, M., and Y. Saito, *Electrotech. J.* (Japan) **2,** 129 (1938); *Sci. Abstr.* **41B**, 526 (1938).
25. Tyler, W. W., and A. C. Wilson, *Phys. Rev.*, **89,** 870 (1953).
26. Eatherly, W. P., and N. S. Razor, U.S. At. Energy Comm. NAA-SR-196 (1952).
27. Kmetko, E. A., *J. Chem. Phys.*, **21,** 2152 (1953).
28. Loebner, E. E., *Phys. Rev.*, **102,** 46 (1956).
29. Mrozowski, S., *Phys. Rev.*, **85,** 609 (1952).
30. Ubbelohde, A. R., and J. Orr, *Nature* **179,** 193 (1957).

31. Blackman, L. C. F., P. H. Dundas, and A. R. Ubbelohde, *Proc. Roy. Soc. (London)* **A255,** 293 (1960).
32. Blackman, L. C. F., G. Saunders, and A. R. Ubbelohde, *Proc. Roy. Soc. (London)*, **A264,** 19 (1961).
33. Klein, C. A., and M. P. Lepie, Raytheon Co., Research Div., September 1963, Tech. Memo T-506.
34. Klein, C. A., Raytheon Co., Research Div., February 1964, Tech. Memo T-552.
35. Mott, N. F., and H. Jones, *The Theory of the Properties of Metals and Alloys*, Dover Publications, New York, 1958.
36. Wilson, A. H., *The Theory of Metals*, Cambridge University Press, London, 1953.
37. Ziman, J. M., *Electrons and Phonons*, Oxford University Press, London, 1960.
38. De Groot, S. R., *Thermodynamics of Irreversible Processes*, Interscience Publishers, New York, 1951.
39. Ziman, J. M., *op. cit.*, 265.
40. Wilson, A. H., *op. cit.*, 6.
41. Mott, N. F., and H. Jones, *op. cit.*, 262.
42. Ziman, J. M., *op. cit.*, 95.
43. *Ibid.*, 92.
44. *Ibid.*, 103.
45. Dekker, A. J., *Solid State Physics*, Prentice-Hall Inc., New Jersey, 1958.
46. Soule, D. E., and J. W. McClure, *J. Phys. Chem. Solids*, **8,** 29 (1959).
47. Thrower, P. A., and W. N. Reynolds, *J Nucl. Mater.*, **8,** 221 (1963).
48. Wallace, P. R., *Phys. Rev.*, **71,** 622 (1947).
49. Mason, I. B., *Industrial Carbon and Graphite*, Society of Chemical Industry, 1958, pp. 60–73.
50. Soule, D. E., *Phys. Rev.*, **112,** 708 (1958).
51. Mrozowski, S., and A. Chaberski, *Phys. Rev.*, **104,** 74 (1956).
52. Walker, P. L., Jr., H. A. McKinstry, and J. V. Pustinger, *Ind. Eng. Chem.*, **46,** 1651 (1954).
53. Franklin, R. E., *Acta Cryst.*, **4,** 253 (1951).
54. Bacon, G. E., *Acta Cryst.*, **4,** 558 (1951).
55. Dawson, I. M., and E. A. C. Follett, *Proc. Roy. Soc. (London)*, **A253,** 390 (1959).
56. *Ibid.*, **A274,** 386 (1963).
57. Rusinko, F., Jr., and P. L. Walker, Jr., *Proc. Conf. Carbon, 4th, Buffalo, 1959*, 751 (1960).
58. Tietjen, J. J., Ph.D. thesis, The Pennsylvania State University, 1963.
59. Borelius, G., *Physikalische Eigenschaften, Handbuch der Metallphysik*, Leipzig 1, 1935, p. 398.
60. *Handbook of Chemistry and Physics*, Chemical Rubber Publishing Company, Cleveland, 1956, p. 2409.
61. Keyes, F. G., and M. J. Marshall, *J. Am. Chem. Soc.*, **49,** 156 (1927).
62. Bull, H. I., M. H. Hall, and W. E. Garner, *J. Chem. Soc.*, 837 (1931).
63. Hine, J., *Physical Organic Chemistry*, McGraw-Hill Book Company, Inc., New York, 1956, p. 34.
64. Cottrell, T. L., *The Strength of Chemical Bonds*, Butterworths Scientific Publications, Ltd., London, 1958, p. 279.

65. Kittel, C., *Introduction to Solid State Physics*, John Wiley and Sons, New York, 1960, p. 293.
66. Soule, D. E., *Proc. Conf. Carbon, 5th, Penn State Univ., 1961*, Vol. **2**, 13 (1963).
67. Redmond, J. P., and P. L. Walker, Jr., *Nature*, **186**, 72 (1960).
68. Kemberling, S. M., M. S. thesis, The Pennsylvania State University, 1963.
69. Savage, R. H., *Ann. N.Y. Acad. Sci.*, **53**, 862 (1951).
70. Glasstone, S., K. J. Laidler, and H. Eyring, *Theory of Rate Processes*, McGraw-Hill Book Company, New York, 1941.
71. Lavrov, N. V., V. V. Korobov, and V. I. Fillipova, *Thermodynamics of Gasification and Gas-Synthesis Reactions*, Pergamon Press, The Macmillan Company, New York, 1963.
72. B. M. W. Trapnell, *Chemisorption*, Butterworths Scientific Publications, London, 1955, pp. 209–216.
73. Samuel Glasstone, *Thermodynamics for Chemists*, D. Van Nostrand Company, Inc., Princeton, 1947, p. 195.
74. Sherman, A., and H. Eyring, *J. Am. Chem. Soc.*, **54**, 2661 (1932).